Salih, E. L., Gardner, L. and Nethercot, D. A. (2010). Numerical investigation of net section failure in stainless steel bolted connections. Journal of Constructional Steel Research. **66(12)**, 1455-1466.

Numerical investigation of net section failure in stainless steel bolted connections

E L Salih; L Gardner; D A Nethercot

Abstract

Despite fundamental differences in the mechanical behaviour of stainless steel and carbon steel, design provisions for stainless steel connections in current standards essentially follow the rules for carbon steel with some limited modifications. For the case of net section capacity, the design rules from EN 1993-1-3 for cold-formed carbon steel have been adopted for stainless steel connections in EN 1993-1-4 and the SCI/Euro Inox Design Manual without any modification. In this paper, an investigation into the behaviour of stainless steel connections failing by net section rupture has been conducted. Numerical models for austenitic and ferritic stainless steel have been developed and validated against existing test results. The validated models were subsequently used to perform parametric studies to investigate the main parameters affecting the net section rupture of bolted connections; these include edge distance e_2 and bolt configuration. By studying the stress distribution along the net section for different edge distances and bolt arrangements, it was found that the ductility of stainless steel is sufficient to ensure extensive redistribution of stresses prior to fracture. Hence, a revised design equation (based on that given in EN 1993-1-3) for net section capacity of stainless steel connections has been proposed and its reliability demonstrated by means of statistical analysis.

Keywords: Bolted connections; Eurocode 3; Finite element modelling; Joints; Net section failure; Stainless steel.

1. Introduction

The use of stainless steel in construction is steadily growing due to its mechanical properties, durability, appearance and fire resistance. A comprehensive explanation of the benefits offered by the material and its usage in structures has been reported by Gardner [1]. Interestingly, although high initial cost is its major drawback, recent developments suggest that low nickel content stainless steel can provide many of the durability related benefits of the more traditional grades but at around half the cost – thereby further encouraging its adoption in appropriate circumstances [2]. Unlike carbon steel, the stress-strain relationship of stainless steel is rounded without a well-defined yield stress and the material exhibits significant strain hardening as shown in Fig. 1. Despite these fundamental differences, design provisions for bolted connections between stainless steel structural members in current international standards are essentially based on the rules for carbon steel with only some very limited modifications [3-6]. This is attributed to the lack of comprehensive information on the behaviour of these particular structural components.

Few studies have been carried out to investigate the behaviour of stainless steel bolted connections. The first experimental work was conducted a quarter of a century ago by Errera et al. [7], where the behaviour of bolted and welded connections was investigated in order to assess the applicability of the design equations for cold-formed carbon steel bolted connections, which had been proposed by Winter [8], to stainless steel. Four failure modes, identical to those reported by Winter were observed. It was concluded that Winter's design equations for net section and bearing resistance were applicable, without modification, to stainless steel connections. Further experimental study of bolted connections between thin gauge ferritic stainless steel elements was carried out by Van Der Merwe [9]. It was concluded that the design provisions for carbon steel connections are suitable for the prediction of tear-out failure and net section rupture in stainless steel connections, but overestimate bearing strength. Most recently, Kim et al. [10] performed tests, together with a numerical study that formed the basis for proposed design equations for net section and bearing for thin gauge stainless steel sheets susceptible to out-of-plane deformations (curling).

The use of stainless steel for main structural components in buildings and bridges – which requires larger thicknesses – encouraged researchers to focus on connections between thicker

hot-rolled plates. The experimental investigation by Ryan [11] was the first study of such connections. Laboratory tests of bolted connections made from three types of stainless steel (austenitic, ferritic and duplex) formed the basis for revising the design provisions in ENV 1993-1-4 [12]. Although Ryan's results suggested removal of the 0.9 reduction factor in the net section resistance formula (which is also employed in the design formula for hot-rolled carbon steel [13]), it was recommended to maintain the k_r factor (employed for cold-formed carbon steel in EN 1993-1-3 [14]) until such time that the number of tests provided full justification for its removal. Bouchair et al. [15] developed numerical models to replicate the behaviour of experimental specimens, and recommended that the reduction factor k_r in the net section design equation and the influence of the end and edge distances on bearing behaviour require further investigation.

In order to improve the design rules for stainless steel connections so as to exploit the differing mechanical characteristics of this material – including high ductility and strain hardening – further investigation is required since the number of test results presently available is limited. In this paper, an alternative approach is adopted in which the available test data are first used to validate numerical models which are then utilised to study a much wider coverage of key design variables. On the basis of the experimental and numerical results, improved design equations for net section capacity of stainless steel connections are proposed.

3. Finite element (FE) modelling

3.1 Material modeling

The stress-strain behaviour of stainless steel differs from that of carbon steel, and representing stainless steel behaviour in FE models using the conventional elastic-perfectly-plastic material model, which is commonly used for carbon steel, leads to inaccurate results. To describe the nonlinear behaviour of stainless steel material, the compound Ramberg-Osgood stress-strain expressions that were developed by Mirambell and Real [16] and Rasmussen [17] – given by Equation 1 – were incorporated in the FE models.

$$\varepsilon = \begin{cases} \dfrac{\sigma}{E} + 0.002\left(\dfrac{\sigma}{\sigma_{0.2}}\right)^{n} & \text{for} \quad \sigma \le \sigma_{0.2} \\ \dfrac{(\sigma - \sigma_{0.2})}{E_{0.2}} + \varepsilon_u\left(\dfrac{\sigma - \sigma_{0.2}}{\sigma_u - \sigma_{0.2}}\right)^{m} + \varepsilon_{0.2} & \text{for} \quad \sigma_{0.2} < \sigma \le \sigma_u \end{cases} \tag{1}$$

where ε is the nominal strain, σ is the corresponding nominal stress, E is the initial Young's modulus, $E_{0.2}$ is the tangent stiffness at the 0.2% proof stress, $\sigma_{0.2}$ is the 0.2% proof stress, $\varepsilon_{0.2}$ is the total strain at the 0.2% proof stress, ε_u is the strain at the ultimate stress f_u and n and m are the strain hardening coefficients.

Since FE analysis for bolted connections is expected to involve large inelastic strains, nominal stresses σ_{nom} and nominal strains ε_{nom} were converted into the corresponding true stresses σ_{true} and true plastic strains ε_{ln}^{pl} respectively. These account for the change of dimensions under load and were incorporated in the models using the following relationships:

$$\sigma_{true} = \sigma_{nom}(1 + \varepsilon_{nom}) \tag{2}$$

$$\varepsilon_{ln}^{pl} = \ln(1 + \varepsilon_{nom}) - \frac{\sigma_{true}}{E} \tag{3}$$

The true stress in a stress-strain curve continues to rise beyond the nominal ultimate stress until the occurrence of fracture. In order to model the full material response until fracture so as to capture the localized stresses and strains, the true stress-strain curve was extended beyond the true ultimate stress up to a fracture strain point of 100% (see Section 3) using Equation 4 [18].

$$\sigma_{true} = K(\varepsilon_{true}^{pl})^{p} \qquad \text{for} \quad \sigma_{u,true} < \sigma_{true} \le \sigma_{frac,true} \tag{4}$$

where $\sigma_{u,true}$ is the true ultimate stress, $\sigma_{frac,true}$ is the true fracture stress, K is the strength constant and p is the strain hardening exponent. K and p were obtained by substituting the true stresses and the corresponding true plastic strains of two points obtained from Equation 1 into

Equation 4. A summary of the values of the constants n, m, K and b for the material employed in this study is given in Table 1. Young's Modulus was taken as 200000 N/mm^2.

All models were developed using the FE package ABAQUS in which material behaviour may be represented by a multi-linear stress-strain curve in terms of true stress and true plastic strain. Plasticity was treated by means of the Von Mises yield criterion with isotropic hardening, whereby the yield surface expands uniformly in all directions such that the yield stress effectively increases in all stress directions as plastic strains develop.

3.2 Element type

The three-dimensional solid element with full integration – C3D8 in ABAQUS – contains eight nodes with three translational displacements for each node and utilises eight integration points. This element is suitable for complex nonlinear analyses involving contact, plasticity and large deformations, and has proved to be suitable when simulating lap bolted connections in previous similar investigations [19, 20] and is hence employed for the models generated herein.

3.3 Contact and bolt preload

Contact between all components that are expected to interact with each other was defined using a surface-to-surface contact command. In this command, two surfaces that may interact with each other are paired; one surface is assigned as a master and the other as a slave. The master-slave algorithm in ABAQUS recognises the surfaces that are in contact and applies constraints (pressure) to slave nodes in order to prevent them penetrating the master surface. The frictional effects between contact surfaces were also included by incorporating the classical isotropic Coulomb friction model in the contact definition, with a friction coefficient μ equal to 0.2, which was used previously in a study by Chung and Ip [19]. The sensitivity to the value of the friction coefficient was also assessed.

The bolt preload which usually arises from bolt tightening has been simulated using the BOLT LOAD option in ABAQUS/Standard. To apply a bolt load using this command a cross-section through the bolt shank and the axis of the bolt shank perpendicular to the cross-section are defined. The total bolt preload value that is acting on the cross-section and

coinciding with the bolt shank axis is then specified. Bolts were located centrally into the holes with a uniform clearance of 1.0 mm. Applied loads were initially carried by friction until the occurrence of slippage after which direct bearing was the primary means of load transfer.

3.4 Method of analysis

A nonlinear structural problem is one in which the stiffness of the structure changes as it deforms. There are three common sources of nonlinearity in structural models, material and geometric nonlinearities being the most frequently encountered; a third source is the boundary nonlinearity associated with a change in the boundary conditions during the analysis. A clear example of this kind of nonlinear behaviour is a model that contains contact between different parts as is the case for bolted connections. In the current study, material, geometrical and contact nonlinearities are incorporated in the models using the PLASTIC, NLGEOM and CONTACT PAIR commands respectively in ABAQUS. A general static analysis with displacement control was employed in the present study. ABAQUS/Standard [21] uses the Newton-Raphson method to obtain solutions for nonlinear problems. In a nonlinear analysis, the solution is found by applying the loads in increments until the final solution. Many iterations may be required to establish a solution at a given load increment. The approximate solution is the summation of all these increments.

Models containing contact definitions are computationally expensive owing to the algorithm that is used to solve these problems. At the beginning of each increment, an inspection of the state of all contact interactions is performed to determine whether slave nodes are open or closed. If the node is closed a further check is performed to identify whether the node is sticking or sliding. Constraints are applied by the algorithm to each closed node and are released from each open node. This process is repeated until no change is found in the status of all slave nodes. Then, an equilibrium iteration is performed, and if the residuals are not within the prescribed tolerance, the increment is neglected and a smaller increment is applied and the procedure is repeated. This process often makes the convergence of such models extremely difficult and in many cases the program terminates due to numerical instability before the entire solution can be found.

3.5 Failure criteria for FE models

To verify the ability of the FE models to replicate the experimental results, including the full deformation characteristics and failure modes, precise material modelling and failure criteria are required. In numerical investigations of structural members such as beams and columns, the ultimate capacity is, simply, the peak load from the load-deformation curve. In the case of bolted connections however, this curve usually exhibits no clear peak; moreover the failure mode must be identified to relate the load carrying capacity to the appropriate mode. For this reason, employing suitable failure criteria is vital when studying bolted connections numerically. Three failure modes were considered in this study – net section fracture, bolt shear failure and bearing failure. The definition of the net section failure in this study is based on a fracture strain criterion – this requires the accurate determination of localized fracture strains in ductile materials, which is discussed below.

3.5.1 Fracture strain determination

The plastic strain at fracture from a tension test coupon based on elongation is given by the following relationship:

$$\varepsilon_{frac,elong} = \ln\left(\frac{L_f}{L_0}\right) \times 100\% \tag{5}$$

where L_0 is the original gauge length and L_f is the final length after fracture. Fracture strains derived using Equation 5 are average values over the chosen gauge length, and will vary with gauge length. This is due to the fact that, for ductile materials, once necking occurs, deformations become localized, resulting in very high strains in a small region until the occurrence of rupture. Dowling [18] explained that for a ductile material Equation 5 significantly underestimates strains beyond necking and therefore is invalid in this region. More accurate values of the true localized fracture strain, which is considered to be more suitable for the prediction of fracture in numerical simulations, can be calculated on the basis of the reduction in cross-sectional area at fracture, as follows:

$$\varepsilon_{frac,red} = \ln\left(\frac{A_0}{A_f}\right) \times 100\% \quad (6)$$

where A_0 is the original cross-sectional area and A_f is the smallest cross-sectional area after fracture.

Many experimental studies have shown that the localized fracture strain obtained using Equation 6 is often much higher than the fracture strain determined using Equation 5. An experimental investigation by Khoo et al. [22] showed that the localized fracture strain based on area reduction for structural carbon steel ranges between about 80% and 120%, with an average value of 100%. Table 2 compares the fracture strains $\varepsilon_{frac,elong}$ and $\varepsilon_{frac,red}$ obtained from test coupons from three studies [18, 23, 24]. Despite marked differences in material properties, the localized fracture strain based on area reduction may be seen to be fairly consistent, ranging between 93% and 113%.

Huns et al. [23] conducted a numerical investigation of gusset plate connections. In validating their FE models a fracture strain of 100% was adopted in the absence of measured values. This value of the localized fracture strain represents a lower bound to their test results and an average of the values reported by Khoo et al. [22].

In the experimental programme on stainless steel connections reported by Ryan [11], the results of which are used in the present study for FE validation, fracture strain of the material based on area reduction was not measured. However, since a number of studies have shown that the localized fracture strain for structural steel and stainless steel based on area reduction are fairly consistent at around 100% (see Table 2), this value will be adopted in the current investigation. In the FE models, fracture of the material was therefore assumed to take place when the plastic strain reached this value.

3.5.2 Net section failure

The existence of holes in a plate causes a discontinuity in geometry and a disruption of the stress trajectories. As a result, stress concentrations occur in the region of the hole. As the applied load increases the magnitude of the maximum stress increases until fracture initiates

at the edge of the bolt hole where the maximum stress concentration develops; the crack then propagates transversely across the net section resulting in the net section failure, illustrated in Fig. 2. The form of this failure is greatly affected by the ductility of the material. If the material is ductile, local yielding at the hole edge as a result of stress concentration allows for stress redistribution at the net section, resulting in necking and finally a ductile failure. In contrast, if the material possesses little ductility, the stress concentration in the vicinity of the hole cannot be redistributed leading to immediate cracking, resulting in a brittle failure. Net section fracture is critical in connections with relatively narrow plate widths. To model net section rupture in the FE models, reference was made to the aforementioned point (see Fig. 2); when the maximum equivalent plastic strain at this point reaches the true localized fracture strain of 100%, it was assumed that a crack initiates, and the ultimate load is said to be reached.

3.5.3 Bolt shear failure

In bearing-type lap connections the load is transferred between the connected plates by means of shear across the bolt cross-section. When the shear load in the bolt exceeds its capacity, a brittle failure occurs called “bolt shear” [25]. Kulak et al. [25] concluded that the shear strength of a single bolt (type A325 and A490) is about 62% of its ultimate tensile strength. Ju et al. [20] investigated bolt shear failure for lap bolted connections similar to those in this study using numerical models. It was proposed that a bolt fails in shear when the critical cross-section of the bolt becomes fully plastic. In the current study, this criterion has also been adopted. Hence, when the equivalent plastic strain over the full critical cross-section reaches the true yield strain, the cross-section of the bolt is fully plastic, and is deemed to have failed. Note that for the test specimens which are used to validate the FE models in the current study, no washers were used, therefore no washers were modelled.

3.5.4 Bearing failure

The bearing resistance of bolted connections may be defined either on the basis of strength or deformation criteria. For the former, the bearing resistance is taken as the maximum load measured in tests regardless of the associated extension. In contrast, adopting a deformation criterion, the ultimate capacity of a connection is defined as the load corresponding to a specified extension. For carbon steel, for which the load-deformation behaviour flattens once

significant bearing deformations have occurred, the exact choice of deformation limit has relatively little effect on the corresponding load. However, stainless steel specimens, owing to the hardening characteristics of the material, generally exhibit a rising relationship, with no clear flattening. Thus, the load level corresponding to bearing failure will depend on the deformation limit selected. Fig. 3 demonstrates the difference in the deformation response for carbon steel and stainless steel bolted connections. In the experimental study performed by Ryan [11], three specimens were reported to have failed in a bearing mode. Since these connections were not loaded until the occurrence of rupture, the reported maximum loads for these connections do not correspond to an actual fracture. Clearly, applying arbitrary deformation limits will give inconsistent results. For this reason, the validation of the FE models for these connections will be on the basis of the load-deformation curves only. The bearing behaviour in stainless steel connections has been investigated by Salih et al. [26] where a true strain-based failure criterion has been used. The distribution of plastic strain in the plate in front of the bolt obtained from parametric studies indicated peak values at two symmetrical locations at about $\theta = 45°$ and 135°, θ being measured from a line through the centreline of the bolt hole(s) perpendicular to the direction of load transfer. This strain distribution accords with observed bearing failures in many tests where fracture initiated at these locations. Salih et al. [26] proposed bearing design equations for two situations, according to the requirement for a deformation limit under service loads. The first equation is for bolted connections where deformation under service loads is not a design consideration. This equation was developed by adopting the strength criterion to define the ultimate bearing capacity, as controlled by fracture. The second equation is for connections where the deformation under service loads is a design consideration, and therefore the equation was developed by considering the deformation allowable under service conditions.

4. Validation of FE models

4.1 Introduction

In this study, the finite element software ABAQUS 6.7.1 [21] was used to develop numerical models for the austenitic grade 1.4306 and ferritic grade 1.4016 stainless steel lap bolted connections that were tested by Ryan [11]. The details of these specimens are presented in Fig. 4 and Table 3.

In order to reduce the size of the model and, consequently, the computational cost, only one quarter of each connection was modelled by applying appropriate boundary conditions. The displacement-control method was adopted, permitting the response beyond the peak load to be followed. A uniform translational displacement was applied at the end of the inner plate. Fig. 5 illustrates the boundary conditions and loading applied to the FE models.

4.2 Comparison between test and FE results

The FE models were validated against the experimental results of Ryan [11] in two steps. In the first step, the overall deformation behaviour was validated by comparing the experimental and numerical load-deformation curves. It should be noted that slip was prevented in the laboratory tests and therefore in all numerical load-deformation curves a slip of 4.0 mm was subtracted from the deformation values. It is clear from Fig. 6 that the predicted load-deformation curves are in good agreement with the tests. The discrepancy in initial stiffness may be attributed to slack in the experimental setup upon first loading. The drop of load after reaching a peak in Fig. 6(a) occurs due to necking of the critical net section; the mode of failure for those models was net section rupture. However, no peak is evident in Fig. 6(b) due to the absence of such necking. Note that the extension shown is the total deformation of the connection, as illustrated in Fig. 7(a). In the second step, the ultimate capacities obtained from the FE models using the proposed failure criteria were compared with those obtained in the tests. The comparison in Table 5 shows that the developed models are able to predict the observed ultimate capacities very accurately, with a mean FE/test ratio of 0.99 and a standard deviation of 0.03. It is shown in Table 5 that the scatter of the results is very low with only 2 tests outside 5%, and 6 tests outside of 2%. The bearing failure reported during testing, as discussed in Section 3, is rather subjective and does not represent a ‘true’ failure and thus it was excluded for the purposes of validation. Comparisons between the deformed specimens for two typical tests and the corresponding FE models are shown in Fig. 7. It can be concluded that the developed numerical models are able to replicate the experimental behaviour and can, therefore, be employed to increase the pool of structural performance data by means of parametric studies.

5. Parametric studies

The number of available test results on stainless steel bolted connections that failed in the net section is insufficient to fully investigate the underlying structural behaviour and to study the effects of the key parameters featured in the design equations, e.g. the edge distance e_2 and the ratio r, which, as described in Section 6, depends on the number and the arrangement of the bolts. In order to investigate these parameters, the data set has been extended by generating further results using the validated FE models. The same two types of stainless steel considered in Section 4 were investigated – the austenitic grade 1.4306 and the ferritic grade 1.4016, though these grades may be considered to be representative of the wider austenitic and ferritic families, respectively, of stainless steel. The material properties of the stainless steels employed in the parametric studies are shown in Table 6. Eurocode 3 Part 1.3 [14] provides design expressions for bolted connections between thin plates with thicknesses of 4.0 mm or less. This definition of thickness range was adopted in the parametric study; 8.0 mm and 10.0 mm thick plates were investigated to represent thick plate connections, while 2.0 mm and 4.0 mm thick plates were considered to represent thin plate connections. To examine the effect of the key parameters (the edge distance e_2 and the ratio r) on the net section capacity of lap connections, six configurations were adopted; these correspond to four values of r (1/2, 1/3, 1/4 and 2/5) with an edge distance ratio e_2/d_0 varying from 1.2 to 4.0 and a constant bolt diameter of 20 mm. The configurations shown in Fig. 8 were adopted for the FE models comprising thin plates (2.0 mm and 4.0 mm), while the configurations of both Figs. 8 and 9 were used for the thick plate models (8.0 mm and 10.0 mm).

6. Design rules for net section failure

6.1 Current design rules

6.1.1 Eurocode 3 and SCI/Euro Inox Design Manual

The design rules for cold-formed carbon steel connections covering net section failure in Eurocode 3 Part 1.3 [14] have also been adopted in Eurocode 3 Part 1.4 [3] and the SCI/Euro Inox Design Manual [4] for stainless steel connections, with no distinction being made

between thick and thin plated connections. Resistance to net section fracture $N_{u,EC3}$ is given by Equation 7:

$$N_{u,EC3} = \frac{k_r A_n f_u}{\gamma_{M2}} \tag{7}$$

where k_r is a reduction factor defined by Equation 8, A_n is the net cross-sectional area at the critical section, f_u is the material ultimate tensile strength and γ_{M2} is a partial safety factor.

$$k_r = 1 + 3r\left(\frac{d_0}{u} - 0.3\right) \leq 1.0 \tag{8}$$

in which d_0 is the bolt hole diameter, r is the ratio between the number of bolts at the cross-section considered to the total number of bolts in the connection and $u = 2e_2$ but $\leq p_2$, where e_2 is the edge distance and p_2 is the spacing between bolts perpendicular to the loading.

6.1.2 ASCE and AS/NZ standards

The ASCE [5] and AS/NZ [6] standards provide design rules for stainless steel bolted connections composed of thin cold-formed sheets, which are similar to those recommended for carbon steel in the AISI Specifications [27]. The nominal net section resistance is given by Equation 9, where symbols have been harmonised with those used in Eurocode 3.

$$N_{u,ASCE} = A_n f_t \tag{9}$$

where, for a single shear connection,

$$f_t = \left(1.0 - r + 2.5r\frac{d}{p_2}\right) f_u \leq f_u \tag{10}$$

and for a double shear connection

$$f_t = \left(1.0 - 0.9r + 3r\frac{d}{p_2}\right) f_u \leq f_u \tag{11}$$

in which d is the nominal bolt diameter, and in the case of single-row bolted connections, p_2 is the width of the sheet.

The design expressions of Equations 8 and 11 are a modified version of Winter's equation [8], which was derived from experiments on bolted connections between cold-formed carbon steel sheets. For specimens failing in net section fracture, Winter concluded that the ductility of this steel, which was less than that of hot-rolled structural steel due to plastic deformation during forming, was not sufficient to overcome the stress concentration effects and redistribute the stresses across the net section. As a result it was concluded that the nominal stress across the net section at failure could not reach the ultimate tensile strength of the material. For bolted connections failing by net section fracture, Winter plotted the ratio of the nominal stress across the net section at ultimate load σ_{net} to the material ultimate tensile strength f_u against d/p_2 ratio, and derived the following equation:

$$\sigma_{net} = k_{r,Winter} f_u \tag{12}$$

where $k_{r,Winter}$ is the reduction factor given by Equation 13.

$$k_{r,Winter} = \left(0.1 + 3\frac{d}{p_2} \right) \tag{13}$$

Popowich [28] also studied cold-formed carbon steel connections and suggested that the reduction factor recommended by Winter [8] accounts adequately for the stress concentration caused by the presence of the hole in the plate but does not distinguish between connections with different numbers of bolts in one row. Popowich [28] concluded that in addition to the basic stress concentration which arises from the existence of a hole in the plate, the application of the bolt load locally at the bolt hole (similar to a point load) is another source of stress concentration and should be considered in the stress reduction factor. Hence, a modification to Winter's formula was proposed, redefining the reduction factor as:

$$k_r = 1 - 0.9r + 3r\frac{d}{p_2} \tag{14}$$

6.2 Proposed design equation

In order to investigate the applicability of the proposals of Winter [8] and Popowich [28] to hot-rolled and cold-formed stainless steel bolted connections, a study of the strain distribution at the critical net section was conducted. The strain distributions obtained from the FE models for connections with the same edge distance e_2 but different r ratios were compared. Fig. 10 shows that the ratio r does not have a significant effect on the strain distribution at the net section at failure in stainless steel connections. A comparison of the strain distribution at the net section at failure for connections with the same r ratio but different edge distances e_2 is shown in Fig. 11. Although the non-uniformity of strain distribution increases with an increase of the edge distance, the ductility of stainless steel is sufficient for the stresses across the net section to be redistributed, thereby eliminating the deleterious effect of stress concentrations.

Fig. 12 and Fig. 13 show the results of the parametric studies for the thick and thin plate connections respectively. It is clear that for stainless steel bolted connections composed of either thick or thin plates failing in net section rupture, the nominal stress at the critical net section (ultimate load / net-sectional area) at failure is consistently greater than or equal to the material ultimate tensile strength. This suggests that the ultimate material tensile strength can be used without including a reduction factor, and hence the ultimate net section capacity $N_{u,prop}$ may be given by:

$$N_{u,prop} = A_n f_u \tag{15}$$

6.3 Statistical validation

In order to verify the net section fracture prediction of Equation 15 and to determine an appropriate partial safety factor γ_{M2}, statistical analyses in accordance with Annex D of EN 1990 [29] were performed. Note that γ_{M2} is the partial safety factor applied in Eurocode 3 Part 1.1 to fracture resistance.

The theoretical design model r_t, which is given by Equation 15, can be written in terms of the basic independent variables as follows:

$$r_t = \frac{t(B - nd_0)f_u}{\gamma_{M2}} \tag{16}$$

where t is the thickness of the plate, B is the width of the plate, d_0 is the bolt hole diameter, n is the number of bolts at the critical cross-section and γ_{M2} is the partial safety factor. The theoretical values of the net section resistance for all the tests are obtained by substituting the actual measured properties into the resistance function in Equation 16. These values are plotted against the corresponding net section capacities from the experiments r_e in Fig. 14(a), while comparisons with both test and FE data are shown in Fig. 14(b). The slope of the least squares regression line b and the coefficient of determination R^2 for both sets are shown in Table 7, for $\gamma_{M2} = 1.0$; the values of b and R^2 being close to unity indicate that the proposed design equation accurately describes the net section failure response.

Material over-strength (the ratio of mean to nominal ultimate tensile strengths) and strength variability, together with variability in geometric properties were accounted for in the statistical analyses. The material over-strength and the material strength variability were taken as 1.20 and 0.027 respectively on the basis of industrial data [30], while coefficients of variation of the geometrical properties were taken, from [31], as follows:

Coefficient of variation for plate thickness $V_t = 0.05$

Coefficient of variation for plate width $V_b = 0.005$

Coefficient of variation for bolt hole diameter $V_{d_0} = 0.05$

The partial safety factor γ_{M2} for the proposed design equation is the ratio between the nominal resistance r_n and the design resistance r_d:

$$\gamma_{M2} = \frac{r_n}{r_d} \tag{17}$$

A summary of the statistical analysis is presented in Table 7, where the following symbols are used: $k_{d,n}$ is the ultimate limit states design fractile factor for n tests, V_δ is the coefficient of variation of the tests relative to the resistance model; and V_r is the combined coefficient of variation incorporating both model and basic variable uncertainties. The maximum required

partial factor, given in the final column of Table 7, for the proposed nominal resistance of the net section is 1.002, hence, it can be safely taken as 1.1, which is less than the recommended value of 1.25 in Eurocode 3 but equal to the value recommended for hot-rolled carbon steel in the UK National Annex to EN 1993-1-1. Therefore, the ultimate design capacity for net section failure of hot-rolled and cold-formed stainless steel bolted connections can be taken as:

$$N_{u,prop} = \frac{A_n f_u}{\gamma_{M2}} \tag{18}$$

where γ_{M2} = 1.1. From Fig. 15 it can be seen that the design provisions for net section failure in Eurocode 3 and the SCI/Euro Inox Design Manual are overly conservative, and the proposed expression provides greater efficiency. Note that, to ensure a ductile failure of a tension member, the ultimate resistance of the net cross-section (Equation 18) should be greater than the yield resistance (gross area × yield strength) of the gross section.

7. Conclusions

Finite element models of stainless steel bolted connections have been developed in this study. Using results from previous laboratory tests, together with appropriate failure criteria, model validation was performed in two stages. Firstly, the load-deformation curves obtained from tests were compared with those extracted from the FE models; excellent agreement was obtained. Secondly, the ultimate capacities were compared; a mean ratio of ultimate FE capacity to ultimate test capacity of 0.99 and a standard deviation of 0.03 was obtained. The validated FE models were used to perform parametric studies to investigate the net section fracture behaviour of stainless steel connections under static shear load. The parametric studies, together with the test data showed that the reduction factor k_r employed in Eurocode 3 Part 1.4 and the SCI/EuroInox Design Manual is unnecessary. A design equation for the net section capacity of stainless steel connections, applicable to both thick and thin material was proposed, and a suitable partial safety factor was derived following reliability analyses in accordance with EN 1990.

Acknowledgements

The authors are grateful to the University of Khartoum (Sudan) and the Prof. Shawki Saad Scholarship for sponsoring this research.

References

[1] Gardner, L. (2005). The use of stainless steel in structures. Progress in Structural Engineering and Materials. 7(2), 45-55.

[2] Theofanous, M. and Gardner, L. (in press). Testing and numerical modelling of lean duplex stainless steel hollow section columns. Engineering Structures.

[3] EN 1993-1-4 (2006). Eurocode 3: Design of steel structures – Part 1.4: General rules – Supplementary rules for stainless steel. CEN.

[4] SCI/Euro Inox (2006). Design Manual for Structural Stainless steel. Third Edition. The Steel Construction Institute and Euro Inox, Building series, Volume 3.

[5] ASCE (2002). Specification for the design of cold-formed stainless steel structural members, SEI/ASCE 8-02. American Society of Civil Engineers. New York.

[6] Aust/NZS (2001). Cold-formed stainless steel structures. Australian Standard/New Zealand Standard AS/NZS 4673. Sydney, Australia.

[7] Errera, S. J., Popowich, D. W., and Winter, G. (1974). Bolted and welded stainless steel connections. Journal of Structural Engineering, ASCE. 100(6), 2549-2567.

[8] Winter, G. (1956). Tests on bolted connections in light gage steel. Journal of Structural Engineering, ASCE. 82(2), 1-25.

[9] Van Der Merwe, P. (1987). Development of design criteria for ferritic stainless steel cold-formed structural members and connections. Ph.D thesis. University of Missouri-Rolla, USA.

[10] Kim, T. S., Kuwamura, H., and Cho, T. J. (2008). A parametric study on ultimate strength of single shear bolted connections with curling. Thin-Walled Structures, 46(1), 38-53.

[11] Ryan I. (1999). Development of the use of stainless steel in construction WP 4.2. ECSC Project No.7210-SA/327.

[12] ENV 1993-1-4 (1996). Eurocode 3: Design of steel structures – Part 1.4: General rules – Supplementary rules for stainless steel. CEN.

[13] EN 1993-1-1 (2005). Eurocode 3: Design of steel structures – Part 1.1: General rules and rules for building. CEN.

[14] EN 1993-1-3 (2006). Eurocode 3: Design of steel structures – Part 1.3: General rules – Supplementary rules for cold-formed members and sheeting. CEN.

[15] Bouchair, A., Averseng, J. and Abidelah, A. (2008). Analysis of the behaviour of stainless steel bolted connections. Journal of Constructional Steel Research. 64(11), 1264-1274.

[16] Mirambell, E. and Real, E. (2000). On the calculation of deflections in structural stainless steel beams: an experimental and numerical investigation. Journal of Constructional Steel Research. 54(1), 109-133.

[17] Rasmussen, K. J. R. (2003). Full-range stress-strain curves for stainless steel alloys. Journal of Constructional Steel Research. 59(1), 47-61.

[18] Dowling, N. E. (1999). Mechanical behaviour of materials. Prentice Hall, New Jersy, USA.

[19] Chung, K. F. and Ip, K. H. (2000). Finite element modelling of bolted connections between cold-formed steel strips and hot rolled steel plates under static shear loading. Engineering Structures. 22(10), 1271-1284.

[20] Ju, S. H., Fan, C. Y. and Wu, G. H. (2004). Three-dimensional finite elements of steel bolted connections. Engineering Structures. 26(3), 403-413.

[21] Hibbitt, Karlsson & Sorensen, Inc (2008). ABAQUS. ABAQUS/Standard User's Manual. Version 6.7-1. Pawtucket, USA.

[22] Khoo, H. A., Cheng, R. J. J. and Hrudey, T. M. (2000). Ductile fracture of steel. Structural Engineering Report No. 233, Department of Civil & Environmental Engineering, University of Alberta, Canada.

[23] Huns, B. B., Grondin, G. Y., and Driver, R. G. (2002). Block shear behaviour of bolted gusset plates. Structural Engineering Report No. 248, Department of Civil & Environmental Engineering, University of Alberta, Canada.

[24] Nip, K. H., Gardner, L., Davies, C. M. and Elghazouli, A. Y. (2010). Extremely low cycle fatigue tests on structural carbon steel and stainless steel. Journal of Constructional Steel Research. 66(1), 96-110.

[25] Kulak, G. L., Fisher, J. W., and Struik, J. H. (2001). Guide to Design Criteria for Bolted and Riveted Joints. Second Edition, published by AISC, copyright by the RCSC.

[26] Salih, E. L., Gardner, L. and Nethercot, D. A. (2009). Bearing failure of bolted connections in stainless steel, Proceedings of the Sixth International Conference on Advances in Steel Structures, Hong Kong.

[27] ANSI/AISI S100-2007. North American Specification for Design of Cold-Formed Steel structural members. American Iron and Steel Institute. Washington, D.C.

[28] Popowich, D. W. (1969). Tension capacity of bolted connections in light gage cold-formed steel. M.Sc. thesis. Cornell University.

[29] EN 1990 (2002). Eurocode: Basis of structural design. CEN.

[30] Groth, H. L. and Johansson, R. E. (1990). Statistics of the mechanical strength of stainless steel sheets, Proceedings of Nordic Symposium on Mechanical Properties of Stainless Steel, Sweden.

[31] Može, P., Beg, D. and Lopatič, J. (2008). Net cross-section design resistance and local ductility of elements made of high strength steel. Journal of Constructional Steel Research. 63(11), 1431-1441.

[32] Kim, H., J. (1996). The effect of end distance on the bearing strength of bolted connections. M.Sc dissertation. University of Texas at Austin, USA.

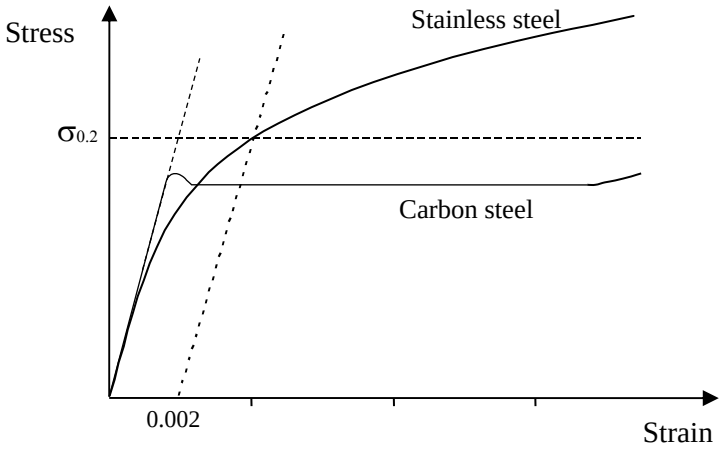


Fig. 1: Stress-strain curves for carbon and stainless steel

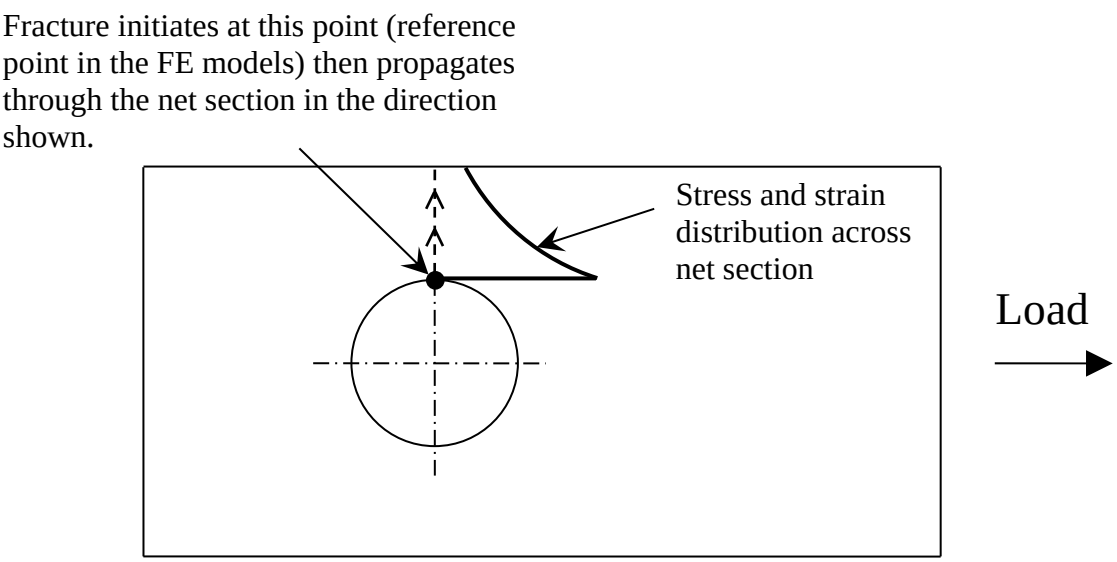


Fig. 2: Illustration of net section fracture

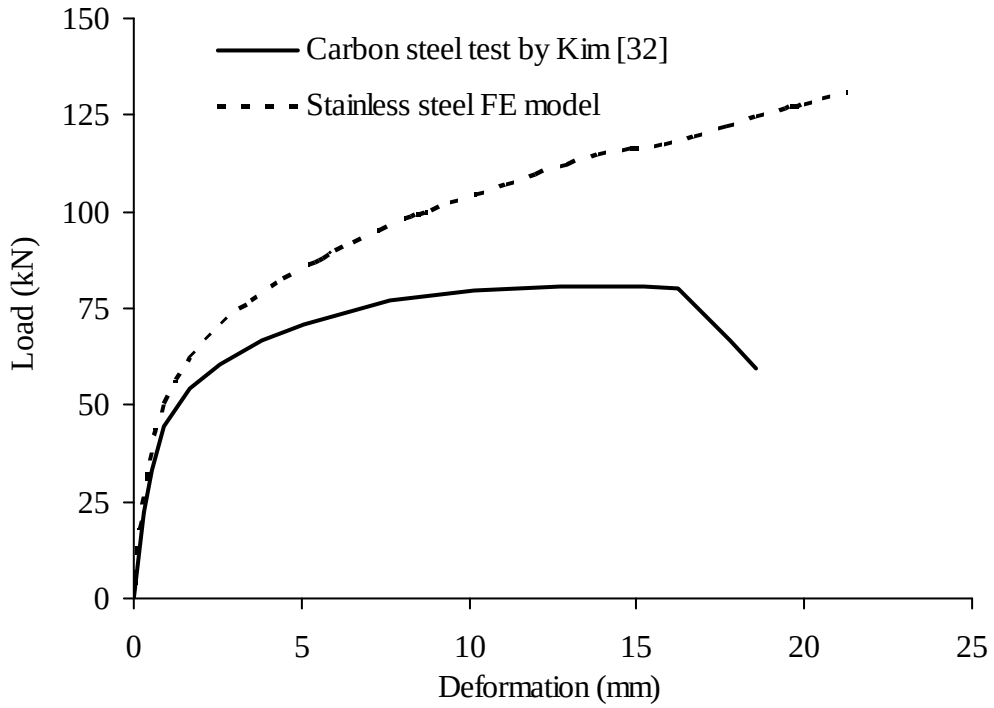
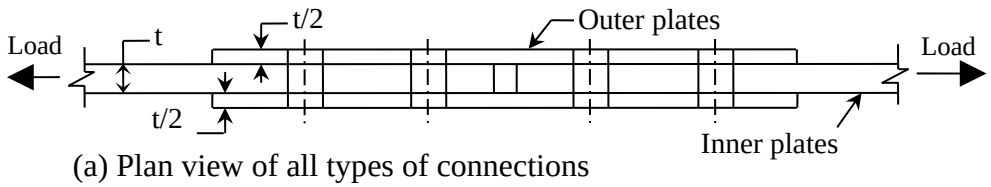
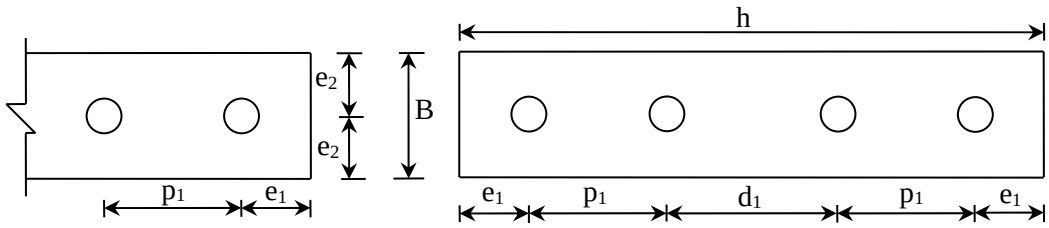


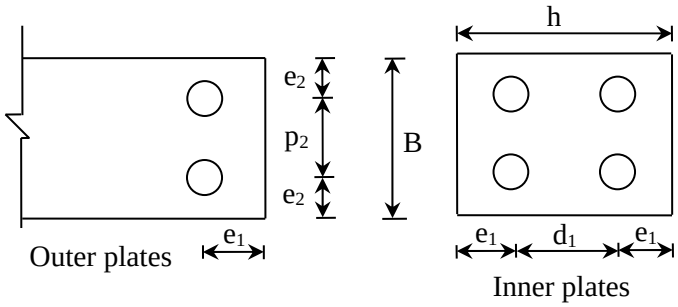
Fig. 3: Bearing behaviour of carbon steel and stainless steel bolted connections with identical geometry



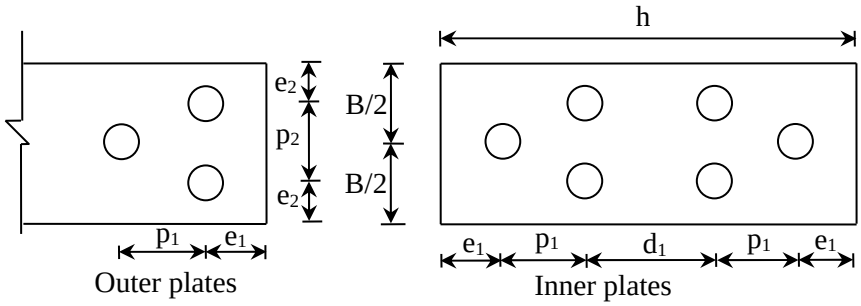
(a) Plan view of all types of connections



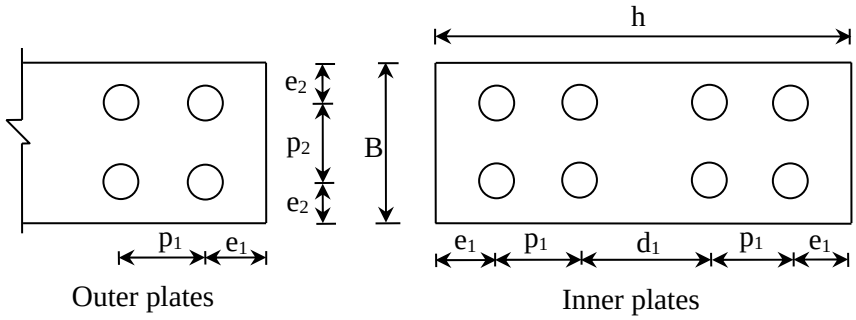
(b) Front view of connection with two bolts longitudinally (type I connections)



(c) Front view of connection with two bolts transversely (type II connections)



(d) Front view of connection with three bolts (type III connections)



(e) Front view of connection with four bolts (type IV connections)

Fig. 4: Configuration of specimens tested by Ryan [11] and investigated numerically in the present study

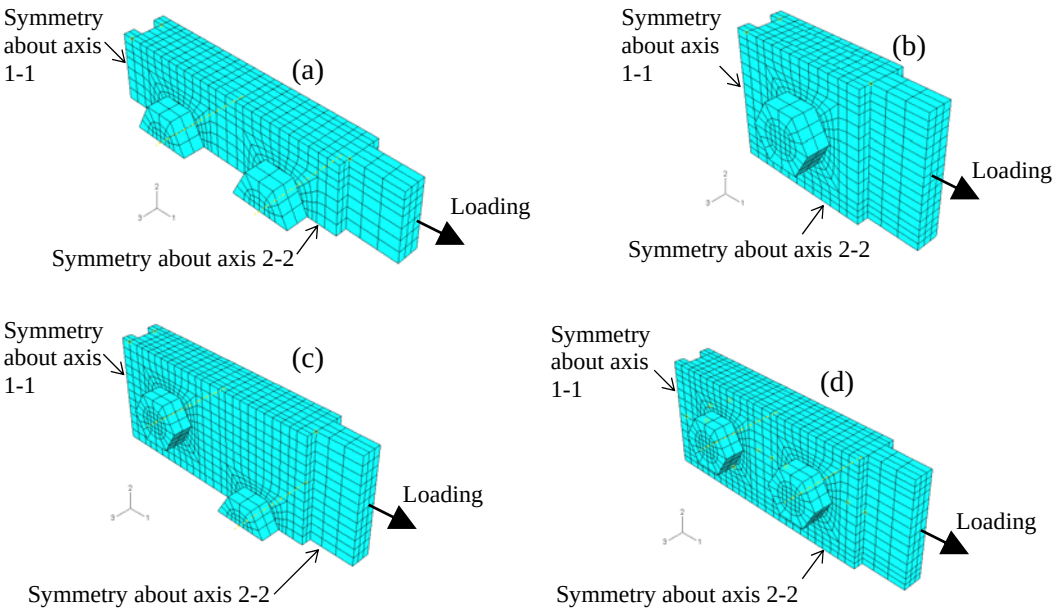
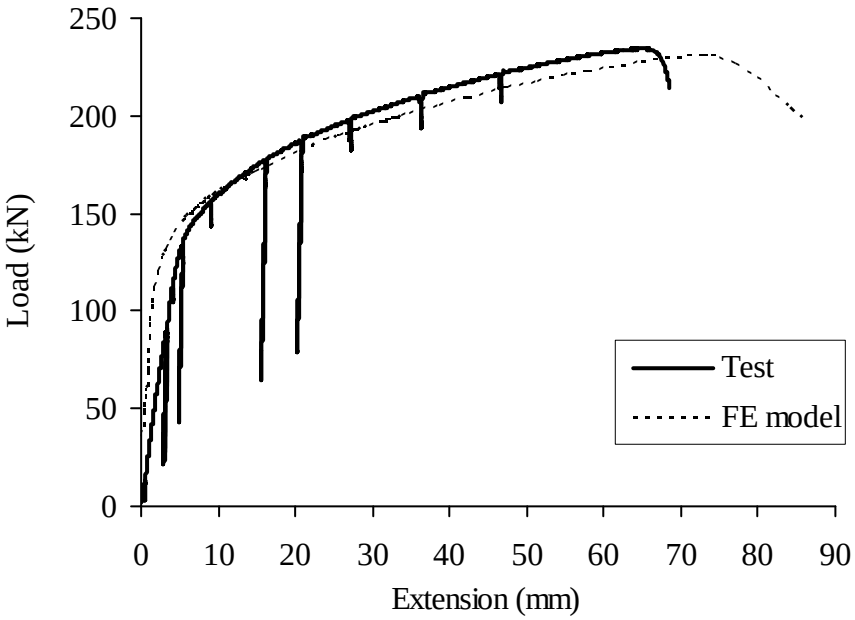
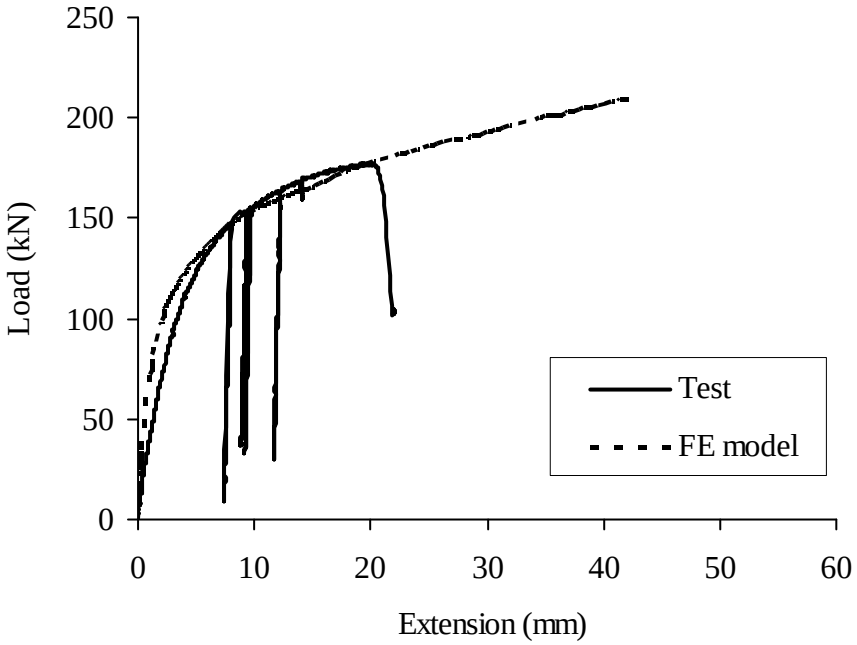


Fig. 5: FE models for the four connection types shown in Fig. 4

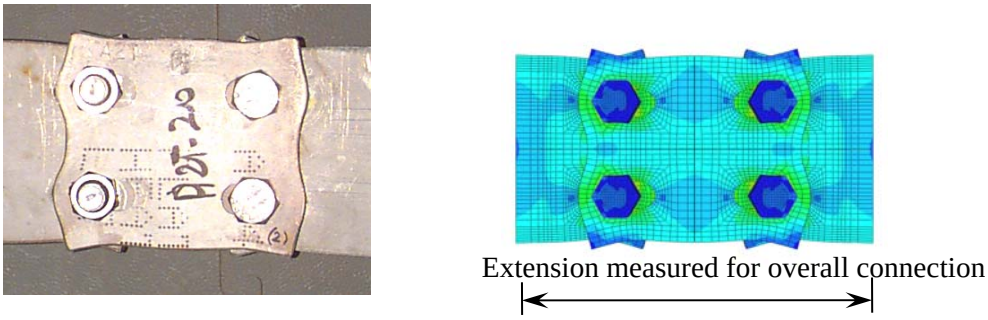


(a) Type I austenitic steel connection

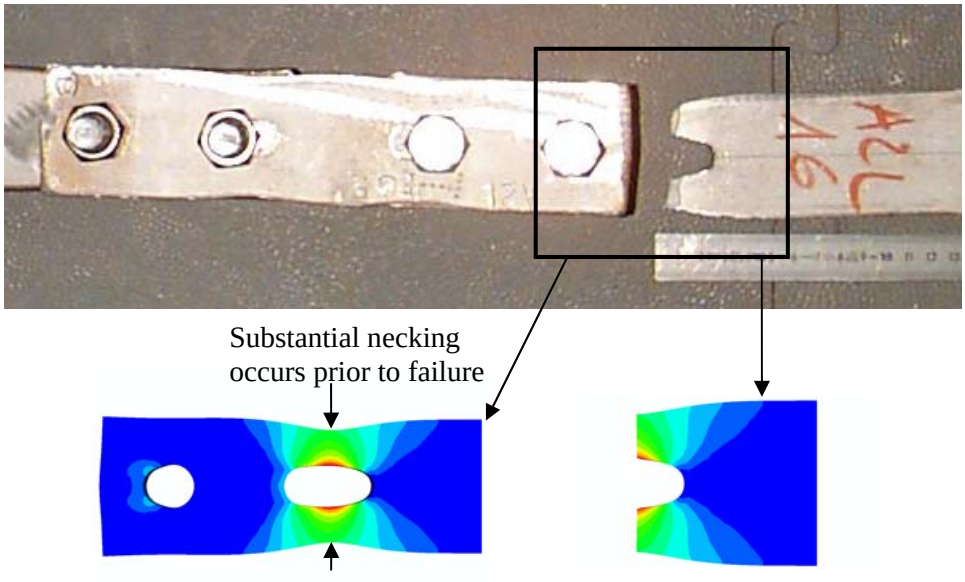


(b) Type II ferritic steel connection

Fig. 6: Typical load-deformation curves from tests and numerical models

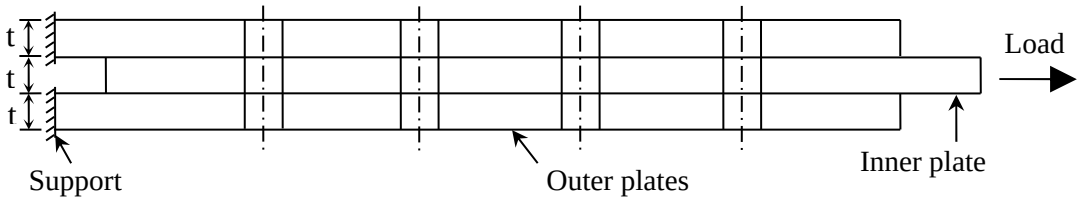


(a): Bearing failure (type I connection)

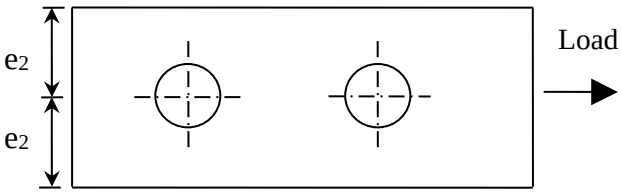


(b): Net section failure (type II connections)

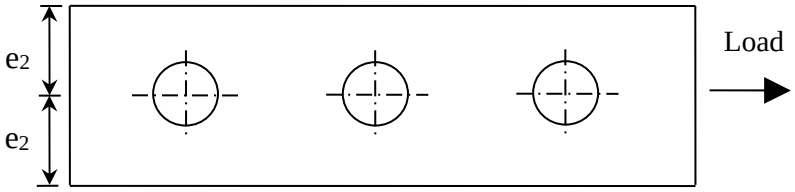
Fig. 7: Comparison between deformed test specimen and numerical model



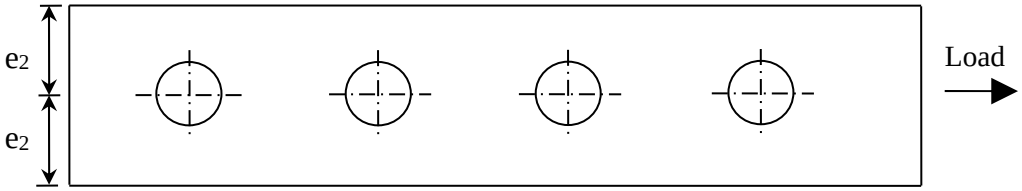
(a) : Plan view



(b): Two bolts

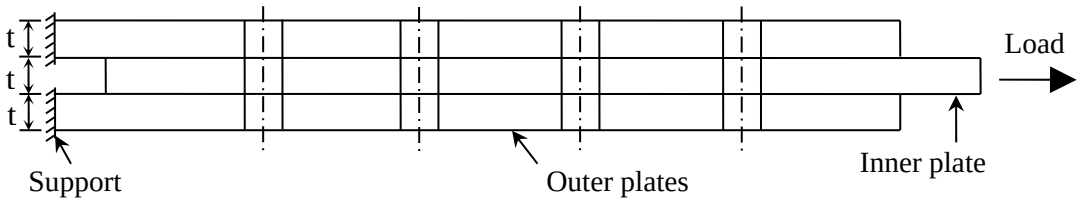


(c): Three bolts

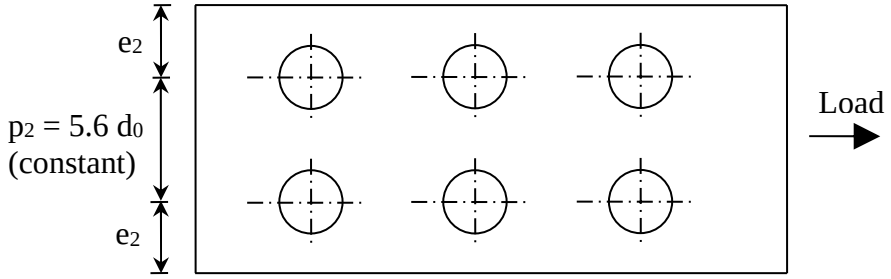


(d): Four bolts

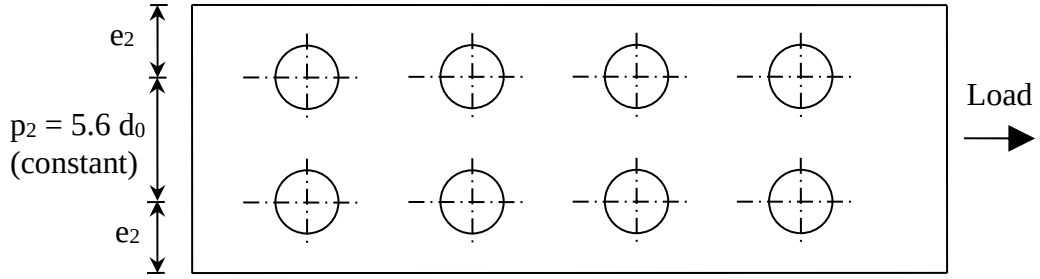
Fig. 8: Single-row bolted connection configuration employed in the parametric studies



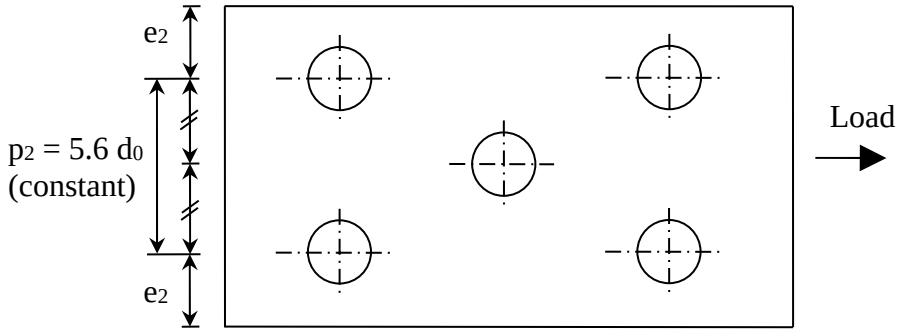
(a) : Plan view



(b): Six bolts



(c): Eight bolts



(d): Five bolts

Fig. 9: Two-row bolted connection configuration employed in the parametric studies

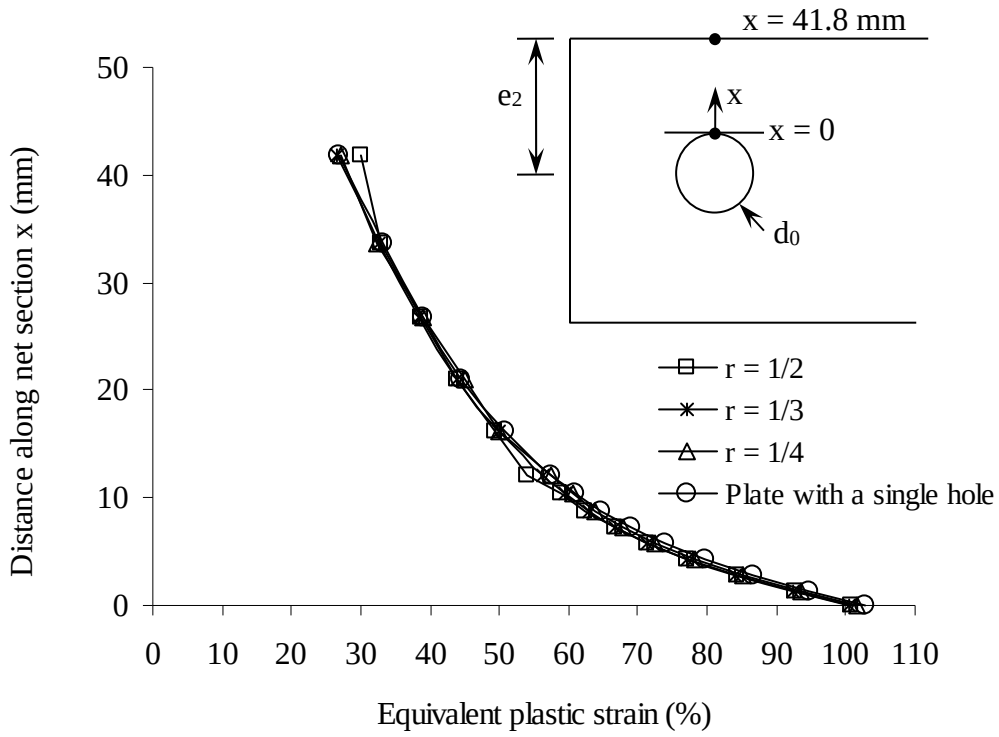


Fig. 10: Strain distribution at failure along net section for austenitic bolted connections with different values of r

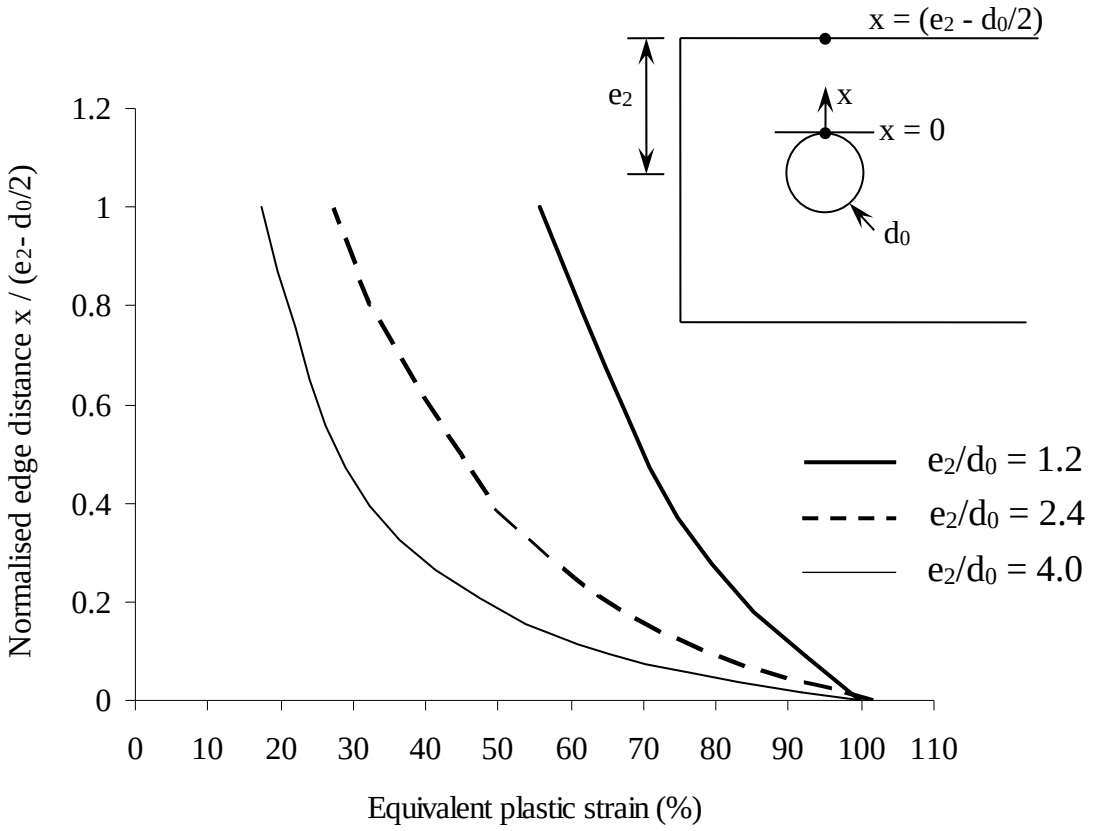
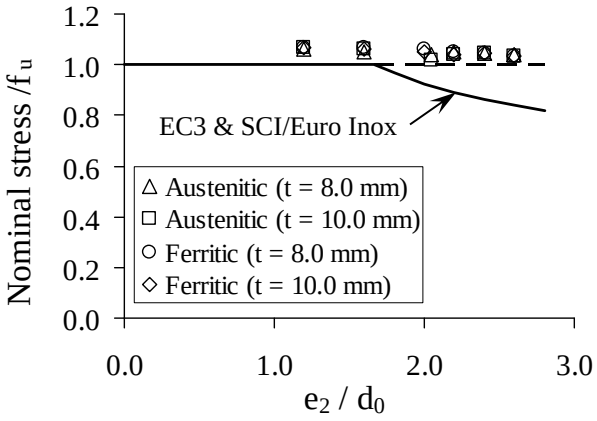
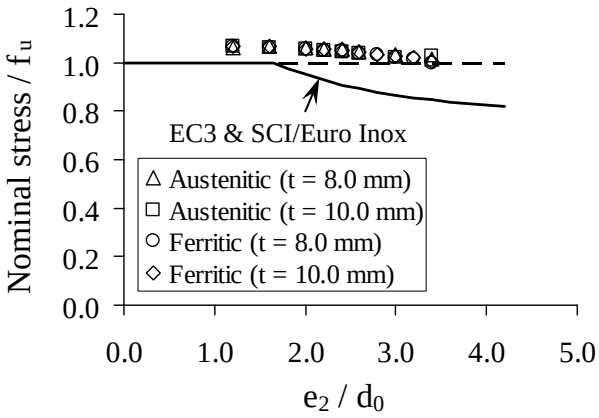


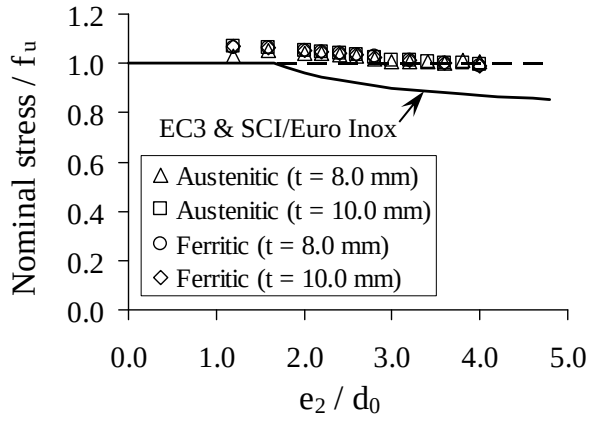
Fig. 11: Strain distribution at failure along net section for single-row austenitic bolted connections with four bolts



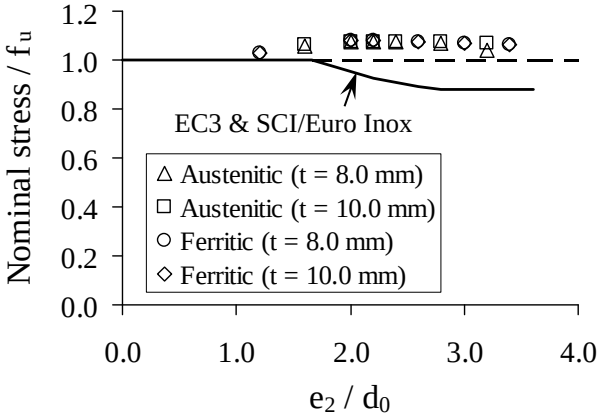
(a): Two bolts in one row



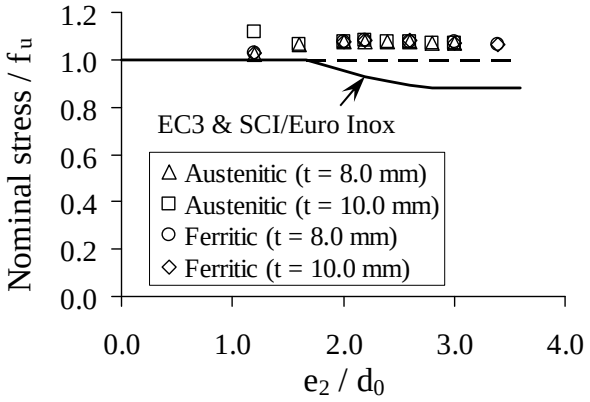
(b): Three bolts in one row



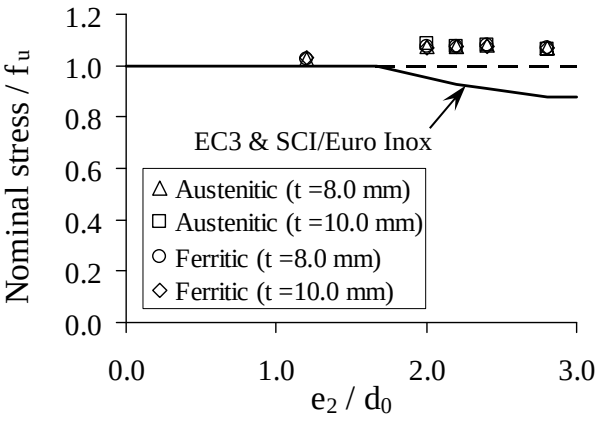
(c): Four bolts in one row



(d): Six bolts in two rows

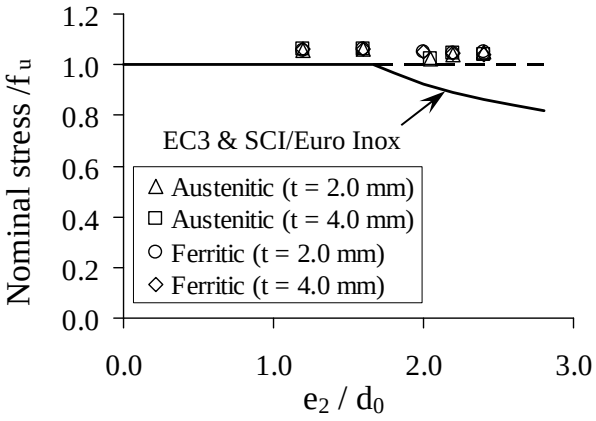


(e): Eight bolts in two rows

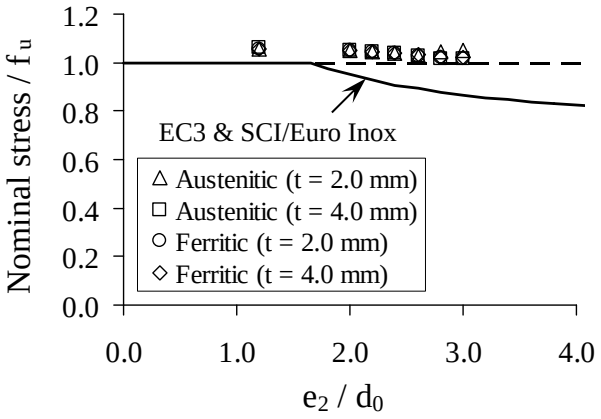


(f): Five bolts

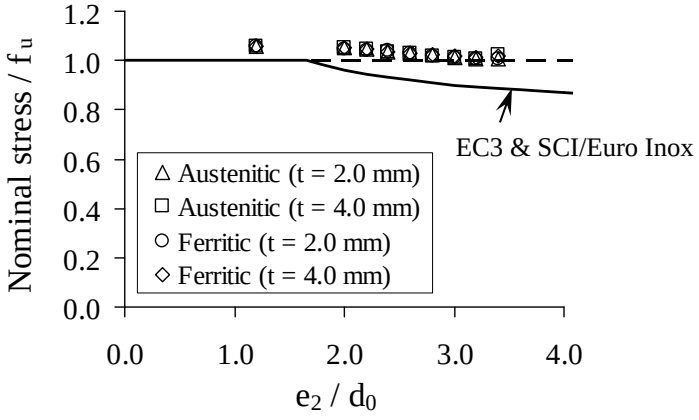
Fig. 12: Comparison between FE model results and codes for bolted connections with thick plates



(a): Two bolts in one row

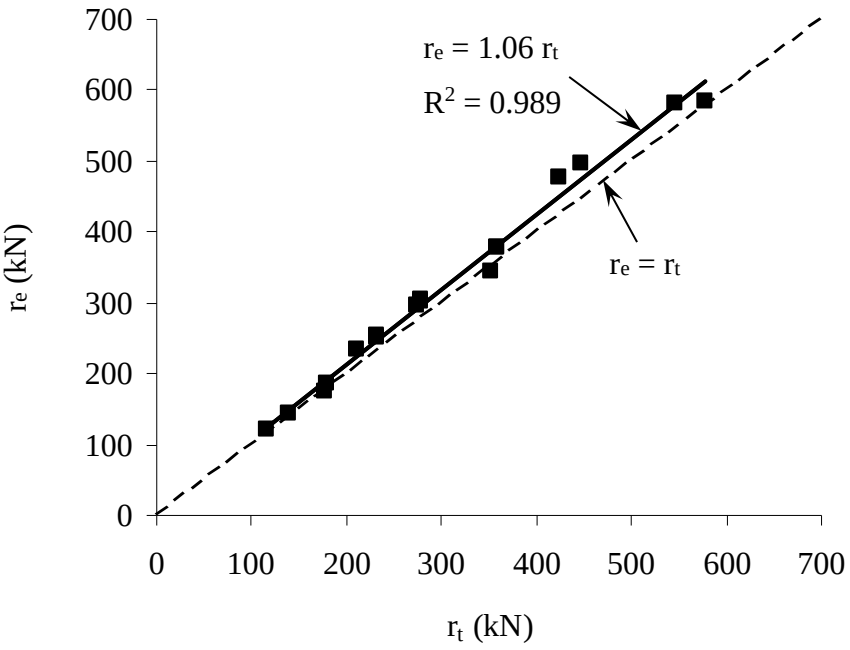


(a): Three bolts in one row

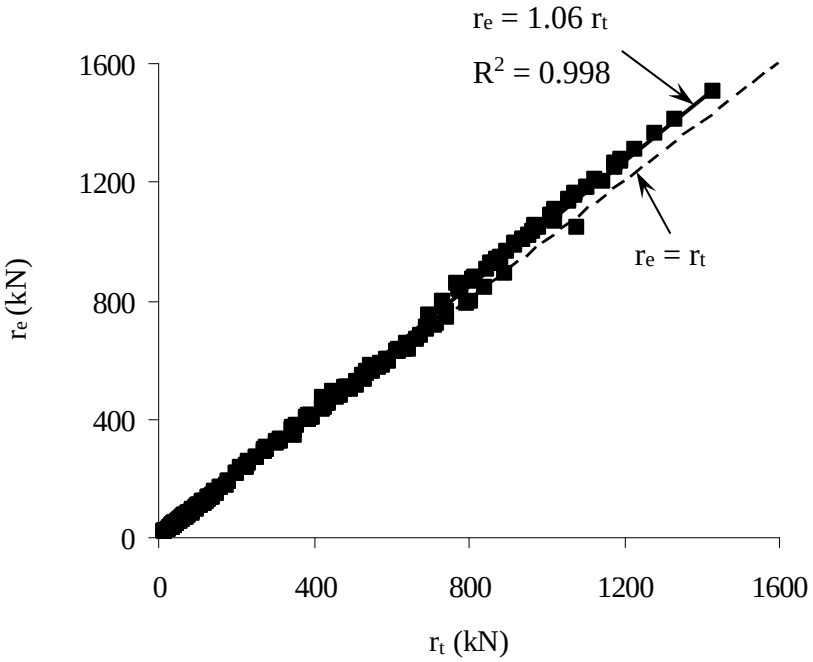


(a): Four bolts in one row

Fig. 13: Comparison between FE model results and codes for bolted connections with thin plates



(a): Test results only [11]



(b): Test results ([11]) and numerical results obtained in the present study

Fig. 14: Comparison between theoretical and experimental or numerical resistances

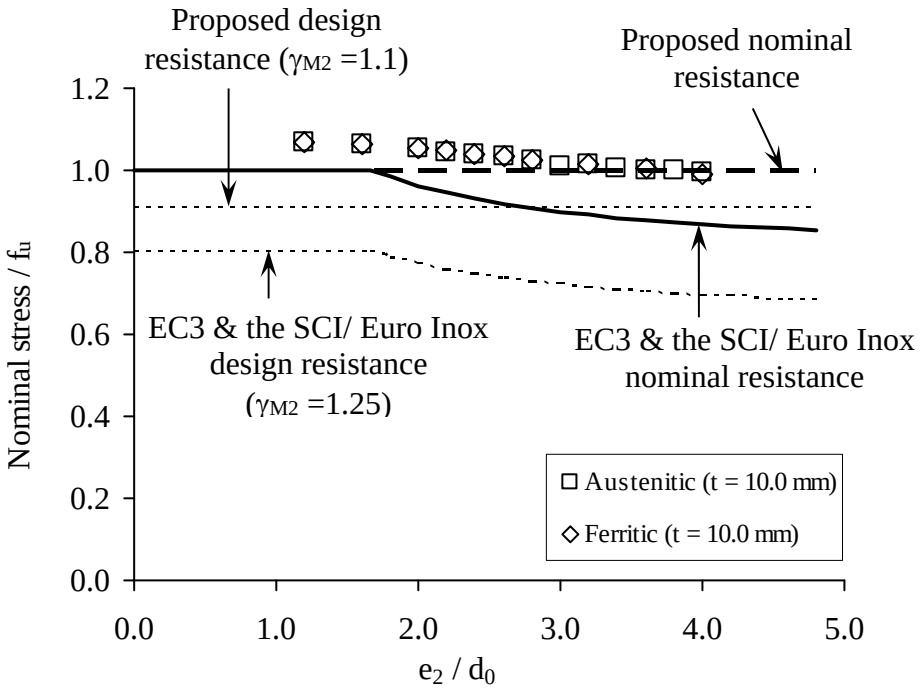


Fig. 15: Comparison between the proposed design equations and those recommended by the Eurocode 3 for connections with four bolts in a single row

Table 1: Coefficients of the material model

Steel	Plates	n	m	K (N/mm^2)	p
Austenitic grade 1.4306	Internal plates	6.58	2.73	1548	0.64
	External plates	6.10	2.64	1585	0.68
Ferritic grade 1.4016	Internal plates	8.16	2.76	1390	0.64
	External plates	12.2	3.50	1008	0.34

Table 2: Coupon test results from existing studies

Ref.	Steel	f_y or $\sigma_{0.2}$ (N/mm^2)	f_u (N/mm^2)	f_u/f_y	$\varepsilon_{frac,elong}$ (%) (Eq. 5)	$\varepsilon_{frac,red}$ (%) (Eq. 6)	$\varepsilon_{frac,red}$ / $\varepsilon_{frac,elong}$
Huns (2002)	Hot-rolled carbon steel	336	450	1.34	26	113	4.34
Dowling (1999)	Hot-rolled carbon steel	260	441	1.70	31	94	3.03
Nip et al. (2010)	Hot-rolled carbon steel	457	547	1.20	31	116	3.74
Nip et al. (2010)	Cold-formed stainless steel	498	755	1.51	47	93	1.98

Table 3: Geometry of experimental specimens [11]

Model No.	Type of connection	Plate material	Bolts diameter (mm)	Plates dimensions (mm)							
				t	e_1	p_1	d_1	e_2	p_2	B	h
1	Type I	Austenitic	12	10	22.5	45	55	22.5	-	45	190
2	Type I	Austenitic	16	10	27.5	55	65	27.5	-	55	230
3	Type I	Austenitic	20	10	35.0	70	80	35.0	-	70	290
4	Type II	Austenitic	12	10	22.5	-	55	22.5	45	90	100
5	Type II	Austenitic	16	10	27.5	-	65	27.5	55	110	120
6	Type II	Austenitic	20	10	35.0	-	80	35.0	70	140	150
7	Type III	Austenitic	12	10	22.5	45	55	22.5	45	90	190
8	Type III	Austenitic	16	10	27.5	55	65	27.5	55	110	230
9	Type III	Austenitic	20	10	35.0	70	80	35.0	70	140	290
10	Type IV	Austenitic	12	10	22.5	45	55	22.5	45	90	190
11	Type IV	Austenitic	16	10	27.5	55	65	27.5	55	110	230
12	Type IV	Austenitic	20	10	35.0	70	80	35.0	70	140	290
13	Type I	Ferritic	12	8	22.5	45	55	22.5	-	45	190
14	Type I	Ferritic	16	8	27.5	55	65	27.5	-	55	230
15	Type I	Ferritic	20	8	35.0	70	80	35.0	-	70	290
16	Type II	Ferritic	12	8	22.5	-	55	22.5	45	90	100
17	Type II	Ferritic	16	8	27.5	-	65	27.5	55	110	120
18	Type II	Ferritic	20	8	35.0	-	80	35.0	70	140	150
19	Type III	Ferritic	12	8	22.5	45	55	22.5	45	90	190
20	Type III	Ferritic	16	8	27.5	55	65	27.5	55	110	230
21	Type III	Ferritic	20	8	35.0	70	80	35.0	70	140	290
22	Type IV	Ferritic	12	8	22.5	45	55	22.5	45	90	190
23	Type IV	Ferritic	16	8	27.5	55	65	27.5	55	110	230
24	Type IV	Ferritic	20	8	35.0	70	80	35.0	70	140	290

Table 4: Material properties of test specimens [11]

Steel	Plates	f_y ($\sigma_{0.2}$) (N/mm^2)	f_u (N/mm^2)	Elongation at fracture (%)	f_u/f_y
Austenitic grade 1.4306	Internal plates	288	581	62	2.02
	External plates	271	577	63	2.13
Ferritic grade 1.4016	Internal plates	262	522	51	1.99
	External plates	350	487	26	1.39

Table 5: Comparison between test and FE results (see Table 3)

Model No.	Type of connection	Plates material	Test		FE		FE/Test
			Ultimate load (kN)	Failure mode	Ultimate load (kN)	Failure mode	
1	Type I	Austenitic	173.9	N/SH	171.6	N	0.99
2	Type I	Austenitic	234.4	N	224.8	N	0.96
3	Type I	Austenitic	297.1	N	289.1	N	0.97
4	Type II	Austenitic	179.4	B/SH	183.6	SH	1.02
5	Type II	Austenitic	341.9	B/SH	328.6	SH	0.96
6	Type II	Austenitic	444.5	B**	-	-	-
7	Type III	Austenitic	269.6	SH	266.7	SH	0.99
8	Type III	Austenitic	496.0	N	477.7	N	0.96
9	Type III	Austenitic	583.6	N**	617.0	N	1.06
10	Type IV	Austenitic	345.6	N/SH	347.2	N	1.00
11	Type IV	Austenitic	475.8	N	465.3	N	0.98
12	Type IV	Austenitic	580.9	N**	598.9	N	1.03
13	Type I	Ferritic	121.0	N	119.0	N	0.98
14	Type I	Ferritic	144.2	N	141.6	N	0.98
15	Type I	Ferritic	187.2	N	183.6	N	0.98
16	Type II	Ferritic	177.5	B/SH	176.3	SH	0.99
17	Type II	Ferritic	211.6	B**	-	-	-
18	Type II	Ferritic	264.8	B**	-	-	-
19	Type III	Ferritic	251.0	N	252.4	N	1.01
20	Type III	Ferritic	301.6	N	298.8	N	0.99
21	Type III	Ferritic	378.3	N	388.1	N	1.03
22	Type IV	Ferritic	254.4	N	250.1	N	0.98
23	Type IV	Ferritic	304.0	N	298.6	N	0.98
24	Type IV	Ferritic	378.7	N	385.6	N	1.02
						Mean	**0.99**
						S.D.	**0.03**

B = Bearing failure - SH = Bolt shear failure - N = Net section failure

** No full rupture occurred during testing

Table 6: Material properties of stainless steel for the parametric studies

Steel	f_y ($\sigma_{0.2}$) (N/mm^2)	f_u (N/mm^2)	Elongation at fracture (%)	f_u/f_y
Austenitic grade 1.4306	288	581	62	2.02
Ferritic grade 1.4016	262	522	51	1.99

Table 7: Summary of statistical analysis results

Data set	Number of tests	$k_{d,n}$	b	R^2	V_δ	V_r	γ_{M2}
Test results	17	3.79	1.06	0.989	0.0403	0.0699	1.002
Test + FE results	278	3.12	1.06	0.998	0.0267	0.0630	0.957